

MATHEMATICAL MODELLING, NUMERICAL SIMULATION AND PARAMETRIC INVESTIGATION OF TRI-COLORED SOLAR THERMAL FLAT-PLATE COLLECTORS FOR TROPICAL CLIMATE

Muhamad-Ali K. Dimapalao^{a,b,*}, Napoleon A. Enteria^a

^aCollege of Engineering, Mindanao State University – Iligan Institute of Technology (MSU-IIT), Tibanga, Iligan City, Philippines

^bCollege of Engineering, Technology and Computing (CETC), Cotabato State University (CotSU), Sinsuat Ave., Cotabato City, Philippines

Article history

Received

28 June 2023

Received in revised form

21 May 2024

Accepted

10 September 2024

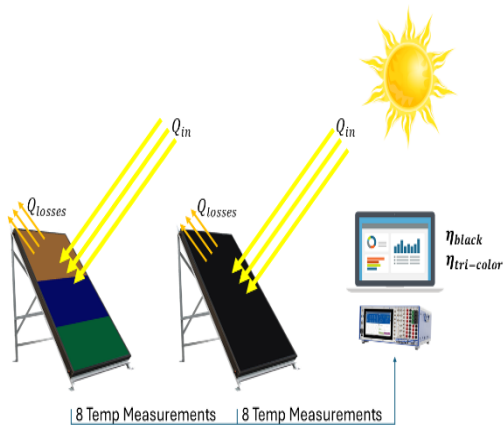
Published online

28 February 2025

*Corresponding author

muhamad-ali.dimapalao@g.msuiit.edu.ph

Graphical abstract



Abstract

The use of non-renewable energy, especially petroleum, has cascading effects that led to the adoption of renewable energy, especially solar energy. One method of using solar energy is through the use of Solar Flat-Plate Collectors (SFPC). Flat-plate solar thermal collectors are often black in appearance due to the hue of the absorbing material, which is used to enhance solar spectrum collection. However, 85% of architects prefer non-black solar collectors, irrespective of their effects on the performance of the system. This study considers the effects of tri-colored SFPC as compared with the black ones. The results show that for three tri-colored collectors, the efficiency could reach as high as 63.57%, just as 16.75% lower than the usual black ones having 80.32% efficiency. This little difference of the tri-colored with the black ones is considerably acceptable especially if we consider their integrations, compatibility with the architectural design and to break away from the dullness of the color black, aesthetically preferable in order to attain a desirable outcome that is both architecturally and visually appealing, as well as aesthetically pleasing and technical integration.

Keywords: tri-colored, solar flat-plate collectors, mathematical modelling, numerical simulation, parametric investigation

© 2025 Penerbit UTM Press. All rights reserved

1.0 INTRODUCTION

The problem that the world is facing on energy exhibits a domino-like effect. Global energy demand is continually increasing, resulting in widespread exploitation of the petroleum-derived fuels, which in turn results to their depletion, and consequently results to the sharp increase in their prices in the world market. This results to the increase of everything, like prices of goods and services in the market. Globally, there are big issues regarding the excessive emission of many internal-combustion engines such as diesel engines which are big contributors to the air pollution and global warming that prompted strict emissions regulations, locally and internationally, for environment protection and public health concerns. These factors led to the use of renewable energy. An

example of renewable energy is solar energy. One of the most commonly used solar energy is solar thermal flat-plate collector. In a recent study on energy, Haque et al. (2021) evaluated the factors influencing energy consumption behavior in urban areas and discovered that there appears to be a positive and linear relationship between income range and energy consumption, indicating that people desire to replace high-energy-consuming appliances as their wealth increases [1].

Simply said, solar flat-plate collectors, or SFPCs, are solar thermal collectors that transfer solar energy into a fluid by absorbing sunlight within a collector. It is appropriate for a wide range of applications where temperatures between 40 and almost 100 °C are required [2]. The flat-panel solar array was invented by Hottel and Whillier in 1950 [2, 3]

Solar flat-plate collectors are black to maximize absorption of solar spectrum by the absorber [4], but which can cause difficulty for building owners and architects when considering their appearance [5]. In contrast with what could happen to the system's efficiency, investigations indicate that 85% of architects would prefer to have solar collectors coated in colors other than black [6, 7, 8]. This research explores the effects of tri-colored SFPC compared with the black ones, and their potential for integration with buildings [7]. By choosing an absorber color that matches the building's facade or roof, a more visually pleasing and architecturally sound design can be achieved [7, 8]. Although these collectors may have lower thermal efficiency due to their lower absorptance compared with black ones, architects find them specially appealing for both modern and traditional buildings [9].

Multiple studies have been performed to assess colored absorbers' efficacy in solar collectors with flat plates. Anderson et al. examined the performance of black, grey, green, red, and white solar collectors [8]. In 2018, Isac, et al. developed red and black absorber coatings for solar thermal collectors, with favorable results [10]. Similarly, Perniu et al., (2020) considered colored flat plate solar thermal collectors, including red, green, and yellow-orange, and recorded nominal efficiencies which are promising [11]. Mueller et al., (2004) observed that the blue- and green-colored absorbers had comparable thermal performance to black solar varnish coated absorbers [12].

In 2014, AlSaqoor, found that, as expected, the average SFPC efficiency employing black and light-gray absorbents was 55% and 12%, respectively [13]. Sakhrieh and Al-Ghandoor (2013) found that metal collectors which have blue and black coatings are more suited for medium- and large-scale use [14]. Isac, et al. studied the colored spectrally coating, including red and gray-green with promising optical performances [15].

According to Zheng et al. (2012), the films that had a purplish pink shade had the highest absorptance, while the films with the orange yellow and purple tints had the lowest emittance [16]. The results of Yang et al.'s (2016) investigation demonstrated that the orange-yellow, purple, blue, blue-green, and yellow-green coatings had solar energy absorptance amounts greater than 0.95 and thermal emissivity quantities lower than 0.09 at 80 °C [17]. Wu et al. (2013) discovered that the coatings' thermal emittance ranged from 0.05 to 0.27 while their solar absorbance varied from 0.82 to 0.94 with the black, red, violet, yellowish-orange, and yellowish-green coatings [18].

Heated water generated from a collector is stored in a separate tank using pipes or tubes. However, there are solar water heating systems with built-in storage tanks, as in the case of the study conducted by Nakoa, et al., (2011), in which, the black absorber obtained a temperature around 54 °C, while the color blue absorber achieved 50 °C in the water [19].

Studies indicate that colored absorbers are slightly less efficient than black ones, due to the latter's higher absorptance. Therefore, some researchers have examined the effects of combining black paint with non-black colors. For example, Orel et al. (2005) mixed a preexisting black paint in different proportions to boost the sun's absorptance of chromatically selective thermal absorber in green, blue, ochre, deeper ochre, and yellow pigment coatings [20]. Another study by Orel et al. (2007) found that green, blue, and to lesser extent red paints coupled selectivity with color. [21]. In their 2000 study, Orel and Gunde mixed black paint with green paint to increase the absorptance in the green layer [22].

There are also some recommendations on how to get the same energy output of colored absorbers with that of black ones. Kalogirou, et al. (2005) found that a proportionately larger collector aperture area for colored absorbers is required to achieve the same energy output as black collectors [9]. Salem suggests a comparable strategy, noting that a two-fold increase (a factor of 2.2) in the collecting area for grey and green absorbers can generate the required amount of energy as with the black one [5].

Another way of increasing the performance and efficiency of colored absorbers is the use of added booster, as shown in the study by Tripanagnostopoulos, et al. (2000), where they added flat booster reflectors into black, blue, and red-brown absorbers, which increased the thermal energy output of the collectors and improved their performance [4]. A further examination into this topic was conducted in 2012 by Zhao, et al., who discovered that adjusting the ratio of oxygen to nitrogen flow may provide a controlled gradient effect throughout the procedure, which increases solar absorptance without compromising the intended color appearance [23].

In this study, four types of solar flat-plate collectors (one black and three tri-colored) will be observed to determine and compare their performances and efficiencies. The tri-colored thermal collectors are preferred configuration in the present study on the point of view of aesthetics and efficiency. A color scheme with too many colors can be difficult to handle and may result in a design that looks overly complex. On the other hand, a design with too few colors can appear dull [24]. Therefore, the researchers aim to incorporate only three colors in the design for three-color combination is a good color scheme and to strike a balance between variation and visual interest, as stated in [25].

In addition, possessing a range of color concepts can prove to be highly beneficial when striving to be trendy in any particular area where color is concerned. However, the more colors you incorporate, the greater the likelihood of things going awry. The adage 'good things come in threes' holds true in this scenario, since there is an exceptional range of color combinations to choose from [26]. Too many colors will deviate from the usual case, that the dark colors especially black have higher efficiency than the lighter ones. Therefore, three (3) colors would be sufficient, so as not to compromise its effectiveness.

There are also many studies conducted on these multi-colored absorbers. In a study by Duta, et al., (2014), they found that Fe_2O_3 hematite pigments were used to obtain bright red spectral selective coatings [27]. Research on chromatically solar selective films for colored flat-surface solar thermal collectors was carried out by Isaac, et al. (2014), and the findings were encouraging [28]. In 2016, Chen, et al. found that all of the considered color units had a solar absorptivity of over 92% and a thermal emissivity of less than 5.5% [29]. In a 2007 study, Orel, et al. found that adding bare aluminum, colored aluminum flake pigments, or copper flake pigments results in low emittance [30].

Wang et al. (2013) investigated the high absorptance, exceeding 95%, of colored solar-thermal absorbing coatings [31]. Similarly, Zhao et al. (2011) obtained an 86% solar absorptance for a single colored-TiAlN-film on an Al substrate [32]. Zhu and Zhao (2010) investigated the black and colored solar-thermal-absorbing coatings with thermal emittance ranges of 0.04 to 0.09 (100 °C) and solar absorptance frequencies of 0.80 to 0.95 [33]. Another study by Dan, et al. (2016), found that by adding more layers, the solar-thermal collectors' color appearance was enhanced, obtaining a low thermal emittance of 0.08 and an

exceptional solar absorptance of 0.948 [34]. Researchers Sarkar et al. (2018) discovered that the colored coatings' solar selectivity is significantly influenced by roughness of the surface, pore density, and size of pores distribution [35].

There are also recent studies on innovations in thermal profiles. In contrast to the control situation, which is when there are no tubercles on the plate, Mu et al. (2020) discovered that plates with tubercles positively influence the flow behaviors under the greatest angle of attack [36]. Additionally, Mu et al. (2020) discovered that the bio-inspired plates' displacements and stresses (which have sinusoidal tubercles) stay below the failure levels [37].

This study considers the installation of solar flat-plate collectors (SFPC) in tropical climates like here in the Southeast Asia (SEA) regions, for the sunlight is mostly available in the whole-year-round. For the past couple of decades or more, there have been changes in the Land Surface Temperature (LST) especially in tropical climate regions. Kamarau et al. (2021) discovered that between 1988 and 2019, marsh and vegetation areas decreased while urban areas rose. The loss of a 5-kilometer square (km²) marsh region resulted in an estimated 1-degree Celsius increase in LST [38].

When deciding colors, one has to carefully consider solar reflectivity (SR) or solar absorptance or absorptivity (α) in addition to the design of the structure. The solar reflectivity, also known as reflectance (SR), of a material is a quantity that ranges from 0 to 100 and indicates its ability to return solar energy from its surface to the atmosphere. A value of 0 (darker color) implies that all of the solar energy is absorbed, while a value of 100 (lighter colors) means that all of the solar energy is reflected. (Houston Steel Buildings, 2020) [39]. Table 1 shows the top five highest solar absorptance color.

So, in this study, the following types of SFPC are considered:

Type A: All Black

Type B: Dark Bronze, Award Blue, Teal Green

Type C: Burgundy, Award Blue, Teal Green

Type D: Burgundy, Award Blue, Dark Bronze

Table 1 Top 5 highest Solar Absorptance color

| Rank | Color | Solar Absorptivity (α) |
|------|-------------|---------------------------------|
| 1 | Award Blue | 82.80 |
| 2 | Teal Green | 71.90 |
| 3 | Dark Bronze | 71.80 |
| 4 | Burgundy | 69.95 |
| 5 | Terra Cotta | 68.34 |

2.0 METHODOLOGY

2.1. Mathematical Modelling

This section presents a mathematical model to explain the transient behavior of an SFPC. The model considers the distinctive qualities in every section of the collection. The five nodes that compose the control volume of consideration in the proposed model, which consists of a single tube, are the transparent covering, air gap, absorbing material, fluid, and insulation. All of these nodes are perpendicular to the line of liquid flow [40, 41, 42], as depicted in Figure 1.

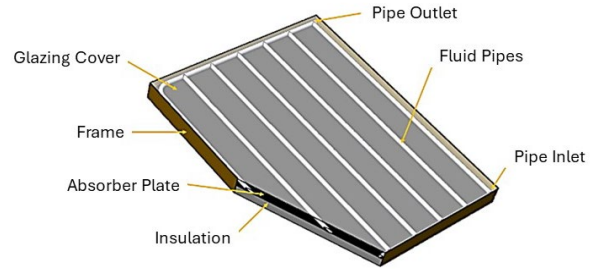


Figure 1 Solar Flat-Plate Collector

The process of developing mathematical and numerical models for flat-plate solar collectors entails capturing the pertinent physical phenomena and their interplay within the collector. This typically involves formulating equations grounded in fundamental principles, integrating suitable boundary conditions, and discretizing the equations for numerical simulations. The steps involved in deriving these models are described in the succeeding paragraphs below. This section details the methodological flow used in the numerical modeling of a solar flat-plate collector, providing a systematic approach to ensure accurate and reliable results.

2.1.1 Identify the Physical Processes

The study begins by identifying the key physical processes occurring within a flat-plate solar collector. These processes include solar radiation absorption, heat conduction through the absorber plate and insulation, convective heat transfer between the fluid and the absorber plate, and radiative heat transfer between the absorber plate, the glass cover, and the surrounding environment. Understanding the interactions and influences of these processes is crucial for accurately modeling the collector's performance.

2.1.2 Formulate the Energy Balance Equation

An energy balance equation is formulated to account for the energy inputs, outputs, and transfers within the collector. This equation balances the energy absorbed from solar radiation against the heat losses through conduction, convection, and radiation, providing a comprehensive description of the energy flow within the collector.

2.1.3 Incorporate Solar Radiation Model

A solar radiation model is developed to estimate the amount of solar radiation incident on the collector surface. This model considers factors such as solar irradiance, collector tilt angle, orientation, and shading effects, providing an accurate estimation of solar radiation intensity at the collector's location and orientation.

2.1.4 Formulate Heat Transfer Equations

Heat transfer mechanisms within the collector are described through the derivation of heat transfer equations. This involves formulating the heat conduction equation to capture heat transfer through the absorber plate and insulation layer. Convective heat transfer equations are included to account for

heat exchange between the fluid and the absorber plate, considering the convective heat transfer coefficient influenced by geometrical arrangement, flow rate, and fluid properties. Radiative heat transfer equations are also incorporated to describe heat exchange through radiation between the absorber plate, glass cover, and surrounding surfaces.

2.1.5 Specify Boundary Conditions

Appropriate boundary conditions are defined to represent the physical conditions at the collector's boundaries. These include the ambient temperature, the fluid's inlet and outlet temperatures, and the amount of solar radiation incident on the collector surface. Boundary conditions provide essential constraints for solving the equations and capturing the collector's behavior under specific operating conditions.

2.1.6 Discretize Equations

Convert the continuous mathematical equations into discrete form to facilitate numerical simulations. Common techniques for discretization include finite difference, finite volume, or finite element methods. Discretization involves dividing the collector into a grid or mesh, approximating derivatives, and converting the equations into algebraic equations suitable for numerical solution.

The mathematical model is structured with a 5 by N node configuration. In this numerical simulation, the equivalent of a mesh domain is achieved through the discretization of the temperature measurements using a specified number of nodes. This process involves dividing the physical domain of the solar flat-plate collector into a grid of discrete points, or nodes, where the governing equations are solved. By using 36 nodes, the simulation captures the essential temperature distributions and heat transfer phenomena within the collector. This discretization ensures that the numerical model can effectively represent the continuous physical processes occurring within the collector, providing reliable data for analysis and optimization.

The visualization in Figure 2 below represents the discretization of the solar flat-plate collector. Each blue "x" mark corresponds to a node where temperature measurements and calculations are performed. The grid provides a structured framework to approximate the continuous physical processes within the collector.

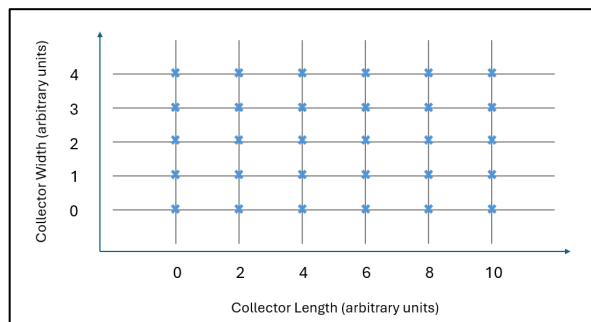


Figure 2 Visualization of nodes in numerical simulations

2.1.7 Solve Numerical Equations

Numerical algorithms and solvers are applied to solve the discretized equations iteratively. This involves solving the resulting system of algebraic equations to obtain temperature

distribution, heat transfer rates, and other relevant variables within the collector. Numerical methods such as Gauss-Seidel, Successive Over-Relaxation, or numerical libraries are utilized to achieve accurate results.

2.1.8 Validate and Optimize the Model

The mathematical and numerical models are validated by comparing the simulation results with experimental data or analytical solutions, where available. Model parameters, such as material properties, geometric configurations, and boundary conditions, are adjusted to improve the agreement between model predictions and experimental observations. The model is iteratively refined and optimized until it adequately captures the behavior of the flat-plate solar collector. This validation ensures the reliability and accuracy of the computed results before conducting a parametric study.

It should be emphasized that the precise characteristics of the mathematical and numerical models for flat-plate solar collectors can differ based on the desired accuracy level, complexity, and the specific assumptions and considerations incorporated during the modeling process. The heat transfer processes within the collector were described in detail by Duffie and Beckman (2013) using energy balance equations. This analysis took into account several elements, including solar radiation, ambient temperature, and collector design characteristics [43]. Kalogirou (2004) emphasized the value of numerical solutions in forecasting temperature distributions and overall efficiency by modeling transient heat transfer in flat plate collectors using finite difference techniques [44]. Additionally, Prakash and Garg (2000) evaluated the performance of tracking and fixed solar collectors using dynamic simulation approaches, emphasizing the effect of temporal fluctuations in solar insolation on collector output [45]. By offering distinct perspectives on the intricate relationships that control solar flat plate collector performance, each of these models helps to improve the technology and applications of these devices.

The energy balance arising from mass transfer throughout the circulation of fluid through a solar collector is taken into account by specifying the temperature of the collector as a function of the location of the coordinates along the fluid flow direction. Using N nodes in the path direction, the model describes the system with (5 x N) nodes. The controlling equations were developed by incorporating the general energy balance for every zone inside the solar collector's control volume [40, 41, 42]. For one-dimensional heat transmission, the overall energy balance is given by

$$\frac{dU}{dt} = \dot{Q}_{in} - \dot{Q}_{out} + \dot{Q}_v \quad (1)$$

where

$\frac{dU}{dt}$ = change in internal energy

\dot{Q}_{in} = heat transfer rate into the system

\dot{Q}_{out} = heat transfer rate out of the system

\dot{Q}_v = heat generation rate into the system.

The glass cover is the outermost part of the flat plate collector. It captures and traps the energy which will be further passed on to the next zones. From the General Equation (1), the energy balance for the glass cover can be presented as:

$$c_g \rho_g V_g \frac{dT_g}{dt} = [h_{g,am}(T_{am} - T_g) + h_{r1}(T_{ab} - T_g) + h_{c1}(T_a - T_g) + \alpha G] p \Delta z \quad (2)$$

where

c = specific heat
 ρ = density
 V = volume
 T = temperature
 t = time
 h = heat transfer coefficient
 α = absorption coefficient
 G = heat flux of solar radiation
 p = tube pitch
 Δz = spatial size of control volume

subscripts:

am = ambient
 g = glass cover
 a = air gap
 ab = absorber
 r = radiation
 c = convection

The air gap is a part of the zones in which energy passes coming from the glass cover and then to the absorber. Eq. (1) can then be modelled for the air gap as:

$$c_a T_a \rho_a T_a V_a \frac{dT_a}{dt} = [h_{c1}(T_g - T_a) + h_{g,ab}(T_{ab} - T_a)] p \Delta z \quad (3)$$

The absorber plays a crucial role in receiving heat in various forms, which is subsequently transferred to the tubes containing the working fluid. It is within this region that the application of multi-colored coatings is considered. In this study, the impact of three different colors of coatings will be examined to assess their overall effect on heat absorption within the absorber zone. This effect is contained in the first term of the right side of the Eq. (4), the values for $\frac{\alpha_1 + \alpha_2 + \alpha_3}{3}$ will be evaluated in later section of this chapter. All forms of energy are modelled as:

$$c_a T_a \rho_a T_a V_a = \left[G \left(\tau \left(\frac{\alpha_1 + \alpha_2 + \alpha_3}{3} \right) + h_{r1}(T_g - T_{ab}) + h_{c1}(T_a - T_{ab}) + \frac{k_i}{\delta_i}(T_i - T_{ab}) \right] p \Delta z + \pi d_{in} h_f \Delta z (T_f - T_{ab}) \quad (4)$$

where

τ = transmittance coefficient
 α = absorption coefficient
 k = thermal conductivity
 δ = thickness
 d = diameter

subscripts:

i = insulation
 f = working fluid
 in = inner

To minimize the useful energy that could leak out of the system, just right next to the absorber an insulation is put in place. The energy balance here is:

$$c_i \rho_i V_i \frac{dT_i}{dt} = \frac{k_i}{\delta_i}(T_{ab} - T_i) + h_{i,am}(T_{am} - T_i) \quad (5)$$

The working fluid is the main energy-capturing device which transports the useful energy to the next components. It will carry

the utilizable portion of the energy flow in the flat-plate solar collector. Eq. (1) for this zone becomes:

$$c_f T_f \rho_f T_f A \frac{\partial T_f}{\partial t} = \pi d_{in} h_f (T_{ab} - T_f) - \dot{m}_f c_f T_f \frac{\partial T_f}{\partial z} \quad (6)$$

where

A = the pipe cross sectional area
 ṁ = working fluid mass flow rate

Lastly, the energy balance for the storage tank is:

$$\frac{dE_{cv}}{dt} = \dot{Q} - \dot{W} + \dot{m}_{in} \left(h + \frac{v^2}{2} + gz \right) - \dot{m}_{out} \left(h + \frac{v^2}{2} + gz \right) \quad (7)$$

These equations for mathematical modelling are based on the equations presented by these authors [7, 8, 40, 41, 42]. These will also be the mathematical bases for numerical method in analyzing the effect of the multi-colored absorber.

2.2. Numerical Simulation

The implicit finite difference method was applied to solve the set of partial differential equations. This method used a forward differential scheme for the temporal derivatives as well as a backward difference strategy for the spatial derivatives in order to discretize them. The forward difference scheme is employed to substitute the time derivatives, in a manner akin to that employed in Ref. [40, 41, 42], viz.

$$\frac{dT_m}{dt} = \frac{T_{m,j}^{t+\Delta t} - T_{m,j}^t}{\Delta t} \quad (8)$$

where m = gc, ag, ab, f, ins, and tank. Updating the dimensional derivatives with a backward difference approach, i.e.,

$$\frac{dT_f}{dz} = \frac{T_{f,j}^{t+\Delta t} - T_{f,j-1}^t}{\Delta z} \quad (9)$$

where:

m = an index of values g, a, ab, f, l
 j = the node number in the flow direction (z)

The final formula of the equation system is [40, 41, 42]:

$$T_{g,j}^{t+\Delta t} = \frac{1}{F_j \Delta t} T_{g,j}^t + \frac{B_j}{F_j} T_{am}^{t+\Delta t} + \frac{C_j}{F_j} T_{ab,j}^{t+\Delta t} + \frac{D_j}{F_j} T_{a,j}^{t+\Delta t} + \frac{E}{F_j} G^{t+\Delta t} \quad (10)$$

$$j = 1, 2, \dots, N$$

$$T_{a,j}^{t+\Delta t} = \frac{1}{H_j \Delta t} T_{a,j}^t + \frac{G_j}{H_j} (T_{g,j}^{t+\Delta t} + T_{ab,j}^{t+\Delta t}) \quad (11)$$

$$j = 1, \dots, N$$

$$T_{ab,j}^{t+\Delta t} = \frac{1}{Q_j \Delta t} T_{ab,j}^t + \frac{K_j}{Q_j} G^{t+\Delta t} + \frac{L_j}{Q_j} T_{g,j}^{t+\Delta t} + \frac{M_j}{Q_j} T_{a,j}^{t+\Delta t} + \frac{O_j}{Q_j} T_{f,j}^{t+\Delta t} + \frac{P_j}{Q_j} T_{i,j}^{t+\Delta t} \quad (12)$$

$$j = 1, 2, \dots, N$$

$$T_{f,j}^{t+\Delta t} = \frac{1}{U_j \Delta t} T_{f,j}^t + \frac{R_j}{U_j} T_{ab}^{t+\Delta t} + \frac{S_j}{U_j \Delta z} T_{f,j-1}^{t+\Delta t} \quad (13)$$

$$j = 1, \dots, N$$

$$T_{i,j}^{t+\Delta t} = \frac{1}{X_j \Delta t} T_{i,j}^t + \frac{V_j}{X_j} T_{ab}^{t+\Delta t} + \frac{W_j}{X_j} T_{am}^{t+\Delta t} \quad (14)$$

$$j = 1, \dots, N$$

$$T_{tank}^{t+\Delta t} = \frac{\dot{m}_{tot} c_p(t_f)}{m_{tank} c_v(t_f)} \Delta \tau (T_{f,n}^t - T_{tank}^t) - h_{tank} \frac{A_{tank}}{m_{tank} c_v(t_f)} \Delta \tau (T_{tank}^t + T_{am}^t) \quad (15)$$

where in the above equations,

$$\begin{aligned} B_j &= \frac{h_{g,am,j}}{c_g \rho_g \delta_g}, & C_j &= \frac{h_{r1,j}}{c_g \rho_g \delta_g}, & D_j &= \frac{h_{c1,j}}{c_g \rho_g \delta_g}, \\ E &= \frac{\alpha}{c_g \rho_g \delta_g}, & F_j &= \frac{1}{\Delta t} + B_j + C_j + D_j, \\ J_j &= c_{ab}(T_{ab})_j \rho_{ab}(T_{ab})_j [p \delta_{ab} + \pi(r_{out}^2 - r_{in}^2)], \\ K_j &= \frac{p(\tau \alpha)}{J_j}, & L_j &= \frac{h_{r1,j} p}{J_j}, & M_j &= \frac{h_{c1,j} p}{J_j}, \\ O_j &= \frac{\pi d_{in} h_{f,j}}{J_j}, & P_j &= \frac{p k_{r1,j}}{J_j \delta}, \\ G_j &= \frac{h_{c1,j} p}{c_q(T_a)_j \rho_a(T_a)_j (p \delta_{ab} + \pi r_{out}^2)}, & H_j &= \frac{1}{\Delta t} + 2G_j, \\ Q_j &= \frac{1}{\Delta t} + L_j + M_j + O_j + P_j, \\ R_j &= \frac{\pi d_{in} h_{f,j}}{c_f(T_f)_j \rho_f(T_f)_j A}, & S_j &= \frac{m_f}{\rho_f(T_f)_j A}, \\ U_j &= \frac{1}{\Delta t} + R + \frac{S_j}{\Delta z}, & V &= \frac{2k_i}{c_i \rho_i \delta_i^2}, \\ W_j &= \frac{2h_{i,am,j}}{c_i \rho_i \delta_i}, & \text{and } X_j &= \frac{1}{\Delta t} + V + W_j \end{aligned} \quad (16)$$

To halt the iteration process in the proposed method, all temperatures must satisfy the specified error criteria:

$$\left| \frac{T_{j,(k+1)}^{t+\Delta t} - T_{j,(k)}^{t+\Delta t}}{T_{j,(k+1)}^{t+\Delta t}} \right| \quad (17)$$

where

- T = is the evaluated temperature in node j
- ϑ = is an acceptable tolerance of iteration (e.g. 10⁻⁴)
- k = 1, 2... is the iteration counter for every single time step

Alongside the termination criterion for the iteration process, the entire procedure must adhere to the Courant-Friedrichs-Lewy stability condition for each time step.

$$|\psi| \leq 1, \quad \psi = \frac{\omega_f \Delta t}{\Delta z} \quad (18)$$

By meeting this requirement, the numerical solution is obtained at a speed $\frac{\Delta z}{\Delta t}$, greater than the physical speed ω_f .

The provided code is a MATLAB implementation of a numerical simulation for a solar collector system. A solar collector is a device that captures and converts solar radiation into usable heat energy, often used for heating fluids or air. The simulation aims to model the temperature distribution and heat transfer within the collector system over a specified time interval. The steps involved

in the numerical simulation are described in the sub-sections below.

2.2.1 Input Parameters:

- n: Number of nodes along the tube (discretization points).
- flowrate: Total flow rate entering the system in liter per hour (LpH).
- interval: Total running time in minutes.
- initialtemp: Initial temperature of the fluid in the tank (degrees Celsius).
- tankvol: Volume of the fluid in the tank in liters.

2.2.2 Initialization and Constants:

The code initializes various constants, such as tube dimensions, fluid properties, and other parameters required for calculations.

ts: Records the CPU time at the beginning of the function.

2.2.2.1 Main Loop:

The simulation iterates over discrete time steps (T_tot) to simulate the behavior of the system over time.

Solar radiation (G_r) and ambient temperature (t_am) are calculated based on time of day. For the first hour, there is solar radiation, and after that, it's zero. The temperature in the surrounding area is consistently at 28 degrees Celsius.

During each iteration of the loop over each time step, the temperature distributions, heat transfer rates, and other variables for every node in the collector are calculated.

2.2.2.2 Temperature Coefficient Calculation:

A function (coeff) is called to calculate various coefficients (B, C, D, etc.) based on temperature values at different nodes (t_g, t_a, t_ab, t_f, t_i) and other parameters.

These coefficients are used in the numerical calculation of temperature changes in the next time step.

2.2.2.3 Temperature Update Loop:

The loop updates the temperature values at each node using the calculated coefficients and temperature values from the previous time step. It checks for convergence, iterating through nodes and calculating errors between current and previous temperature values. If the errors are below a certain threshold, the node is considered converged.

2.2.2.4. Results and Output:

The code stores various temperature profiles (t_gc, t_ac, t_abc, t_fc, t_ic, t_out, t_tank), heat transfer rates (Q_dot), and other parameters.

It outputs the results to a file named ptemp.out and displays progress and convergence information during the simulation.

2.2.2.5 Plotting:

After the simulation, the code uses MATLAB's subplot and plot functions to visualize the results.

It creates multiple subplots to display temperature profiles, temperature changes over time, heat transfer rates, and solar radiation.

2.2.2.6 Runtime Calculation:

The total runtime of the simulation is calculated by subtracting the CPU time at the beginning from the current CPU time.

2.2.2.7 Function Definitions:

The code contains several functions (coeff, get_constants, get_h, air_prop, rho, kf, waterprop) that are called within the main simulation loop to perform specific calculations.

In summary, this code simulates the behavior of a solar collector system by numerically solving heat transfer and fluid flow equations over discrete time steps. It calculates temperature distributions, heat transfer rates, and other parameters within the collector and displays the results using MATLAB plots. The simulation is complex and involves a deep understanding of heat transfer, fluid dynamics, and numerical methods to fully comprehend and modify. Figure 3 shows the code flow chart.

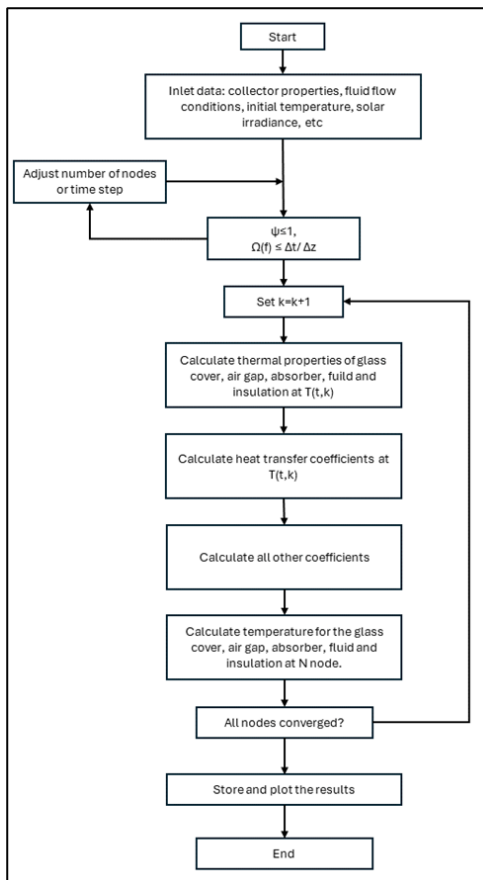


Figure 3 Code flow chart

2.3. Parametric Investigation

The System Advisor Model (SAM), designed by the National Renewable Energy Laboratory (NREL), a branch of the U.S. Energy Department, is utilized in this study's parametric analysis. An open-source, techno-economic software model this helps

decision-makers in the renewable energy sector. Project directors, engineers, incentive system developers, technology developers, and academics are among the people in the renewable energy business who can benefit from an economic and performance model of this SAM. It forecasts the performance of geothermal, wind, biomass, grid-connected solar PV, and concentrated solar power systems [46].

2.3.1. Inputs

From SAM, we choose Solar Water Heating, then No financial model. From there, it has two (2) components: (1) Location and Resource, and (2) Solar Water Heating. Then, the Parametrics. Under Solar Water Heating, the following are chosen for Inputs:

Inputs:

1. Azimuth {'azimuth'} (deg)

The array's east-west orientation in degrees. An azimuth value of 180° is facing south in the northern hemisphere. As a rule of thumb, system designers often use an array azimuth of 180°, or facing the equator [47].

2. Collector area {'user_area_coll'} (m²)

For simplicity, one solar flat-plate collector (SFPC) for each type (Types A – D) is designed to be used by a single person domestically. The length of the collector is 1 m and its width is 0.80 m, for the area of the collector equal to 0.80 m². Accordingly, you will need about 10 to 16 ft² (0.93 to 1.49 m²) of flat plate collector area per person [48]. For tropical climates like Philippines, a minimum of 0.8 m² will do.

3. Pipe diameter {'pipe_diam'} (m)

From Rathi (2016), for solar water heater model selected with a natural circulation type, the water mass flow rate that can be considered is 0.01667 kg/s or 0.264 gpm [49]. So, for 0.264 gpm, from Table 2 below, provided by Solar365 (2024) [50] we use a 1/2" - diameter pipe, or 0.0127 m.

Table 2 Pipe size with respect to maximum flow (Solar365, 2024)

| Pipe Size | Recommended Maximum Flow |
|-----------|--------------------------|
| 1/2" | 1 1/2 gpm |
| 3/4" | 4 gpm |
| 1" | 8 gpm |
| 1 1/4" | 14 gpm |
| 1 1/2" | 22 gpm |
| 2" | 45 gpm |
| 2 1/2" | 85 gpm |
| 3" | 130 gpm |

4. Pipe insulation thickness {'pipe_insul'} (m)

The pipe insulation thickness is solved using the formula for steady-state heat transfer through insulating material wrapped around a pipe as follows [51]:

$$Q = 2\pi kN \frac{(T_o - T_i)}{\ln(R_i/R_p)}$$

where

Q = Total heat transferred / Allowed heat loss (in W)

k = Thermal conductivity of insulating material
= 0.033 W/(m·K) {for rubber insulation [52]}

N = Length of pipe
= 1 meter (m)
 T_p = Operating temperature of fluid inside pipe
= 85 °C
 T_i = Maximum temperature allowed on the outside surface of insulation
= typically 50 °C [51]
 R_p = Radius of pipe
= Pipe Diameter / 2
= ½ (¾) in.
= 0.375 in. = 0.009525 meters (m)
 R_i = Radius of insulation (in m)

From The Engineering ToolBox [53], the insulated copper tubes heat loss per meter for ¾ - in tube is
 $Q/N = 8 \text{ W/m}$

Thus,

$$Q = 2\pi k \frac{(T_p - T_i)}{\ln(R_i/R_p)}$$

$$8 = \frac{2\pi (0.033) (85 - 50)}{\ln(R_i/R_p)}$$

$$\ln(R_i/R_p) = 0.907$$

$$R_i = R_p \times e^{0.907}$$

$$= (0.009525)(2.48)$$

$$= 0.0236 \text{ m}$$

Hence, insulation thickness (t) = $R_i - R_p$
 $t = 0.0236 - 0.009525$
 $= 0.01407 \text{ m or } 14.07 \text{ mm}$

5. Solar tank height to diameter ratio {'tank_h2d_ratio'}

Defines as the solar storage tank geometry, and by extension its geometry [47].

In many studies and publications of standard organizations, such as by Comaklı et al. (2012), it is advised that the rate of storage tank volume to collector area can be between 50 and 70 L/m² [54].

$$\text{Tank Volume } (V_T) = (70 \text{ L/m}^2) \times \text{Collector Area}$$

$$= (70 \text{ L/m}^2) \times 0.8 \text{ m}^2$$

$$= 56 \text{ L}$$

The tank has the following dimensions:

Height (H) = 20 in
 Length (L) = 15 in
 Width (W) = 12 in

$$\text{Thus, Height-To-Diameter (h2d) ratio} = 20/13.5$$

$$= 1.48$$

6. Solar tank maximum water temperature {'T_tank_max'} (°C)
 As from above, Comaklı et al. (2012), in many studies and publications of standard organizations, it is advised that the temperature of the usable water could be between 45 and 60 °C. So, 60 °C will be enough [54].

7. Solar tank volume {'V_tank'} (m³)

From above, item No. 5. The tank volume (V) is
 $V = 58.99 \text{ liters (L)}$

8. Tilt {'tilt'} (deg)

The tilt is array's tilt angle in degrees from horizontal. As a rule of thumb, system designers often use the location's latitude as the optimal array tilt angle [47, 55, 56]. And, for maximum annual energy, the collectors should be tilted towards the equator, i.e. towards the south in the northern hemisphere and north in the southern hemisphere [57].

The experiments were conducted at the rooftop of College of Engineering and Technology (COET) Building at Mindanao State University (MSU) - Iligan Institute of Technology, Tibanga, Iligan City, Philippines (coordinates: latitude and longitude: 8.2280° N, 124.2452° E).

Thus, since the Philippines is located in the northern hemisphere, the collector has faced south and inclined with an angle of inclination of $\phi = 8.2^\circ$ equal to the local latitude of the location.

9. Total piping length in system {'pipe_length'} (m)

The SFPC has dimensions of 1 m x 0.8 m. There will be seven (7) tubes that are vertically soldered into the absorber.

$$\text{Total piping length} = 7 (1 \text{ m}) + 2 (0.8 \text{ m}) + 1 \text{ m (from absorber to tank)} + 2 \text{ m (from tank back to absorber)} = 11.6 \text{ m}$$

10. Total system flow rate {'mdot'} (kg/s)

From Rathi (2016), for solar water heater model selected with a natural circulation type, the water mass flow rate that can be considered is 0.01667 kg/s [49].

There are five (5) runs in the Simulation. The input values are shown in Table 3. The values for each run were played at

Table 3 Inputs for Parametric Investigation

| Run | azimuth (deg) | user_area_coll (m ²) | pipe_diam (m) | pipe_insul (m) | tank_h2d_ratio (l) | T_tank_max (C) | V_tank (m ³) | tilt (deg) | pipe_length (m) | mdot (kg/s) |
|-----|---------------|----------------------------------|---------------|----------------|--------------------|----------------|--------------------------|------------|-----------------|-------------|
| 1 | 178 | 0.76 | 0.0115 | 0.0135 | 1.35 | 58 | 0.0575 | 8.0 | 10.5 | 0.015 |
| 2 | 179 | 0.78 | 0.012 | 0.014 | 1.4 | 59 | 0.058 | 8.1 | 11 | 0.016 |
| 3 | 180 | 0.80 | 0.0127 | 0.0147 | 1.48 | 60 | 0.0589 | 8.2 | 11.6 | 0.01667 |
| 4 | 181 | 0.82 | 0.013 | 0.015 | 1.5 | 61 | 0.059 | 8.3 | 12 | 0.017 |
| 5 | 182 | 0.84 | 0.0135 | 0.0155 | 1.55 | 62 | 0.0595 | 8.4 | 12.5 | 0.018 |

Thus, the volume (V) will be:

$$V = H \times L \times W = (20)(15)(12)$$

$$= 3,600 \text{ in}^3 = 58.99 \text{ L}$$

$$\text{Diameter (D)} = \frac{(15 + 12)}{2} = 13.5$$

2

deviations of at most $\pm 5\%$ of the solved parameter, to determine the study of the influence of different geometric or physical parameters or both on the solution of the problem.

3.0 RESULTS AND DISCUSSION

3.1. Numerical Simulation Results

Figures 4 - 7 show the results of the Numerical Simulation. For each of the four figures, the upper left shows the temperatures of the SFPC, upper right shows the temperatures of the fluid, lower left shows the heat obtained, and lastly, the lower right shows the efficiency.

The symbols used in Figures 4 - 7 refer to the following:

t = temperature
Q_dot = heat obtained

subscript;

t_gc = glass cover
t_ac = air gap
t_abc = absorber
t_fc = fluid
t_ic = insulation
t_amb = ambient
t_in = inlet
t_out = outlet
t_fc = fluid

For every temperature measurement, a maximum of 72 nodes can be used to increase accuracy. This can be done to guarantee excellent resolution and precision when recording the solar flat-plate collector's temperature distribution and heat transfer phenomena. However, 36 nodes were chosen in order to simplify the model while preserving a respectable degree of accuracy. And during the runs, 36 nodes were the common number of nodes that all trials converged. For some runs, increasing the number of nodes led to diverging results. Hence for uniformity in accuracy, 36 nodes were chosen.

From Figure 4, for the Type A, on the upper left, which are the absorber temperatures, the sequence of the temperatures (from highest to lowest) is: absorber (313.8 K), fluid, air gap, insulation, ambient, glass cover. On the upper right side, which are the temperatures of the fluid, the sequence of the temperatures from highest to lowest is: out (313.8 K), fluid, in. And, on the lower left, the highest heat obtained is almost 1,000 watts (W). And lastly, on the lower right side, the efficiency reaches 80.32%.

From Figure 5, the results obtained for Type B are similar to those of Figure 4. This means that the sequence of temperatures from highest to lowest on the upper left (absorber temperatures) is as follows: absorber (310.9 K), fluid, air gap, insulation, ambient, and glass cover. On the upper right side (fluid temperature), the sequence of temperatures from highest to lowest is: out (310.9 K), fluid, and in. The highest heat obtained on the lower left is nearly 800 watts (W). Lastly, the efficiency on the lower right side reaches 63.57%.

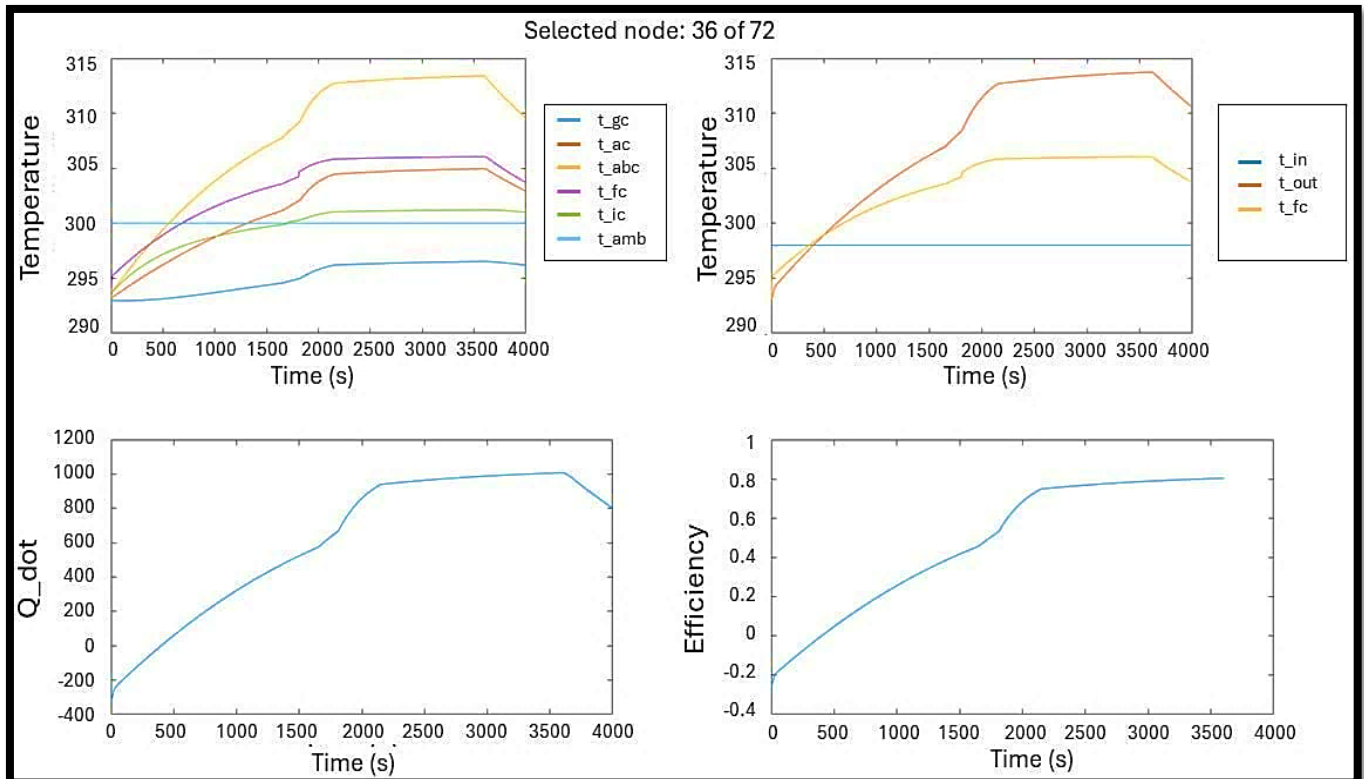


Figure 4 Type A: eff = 0.8032

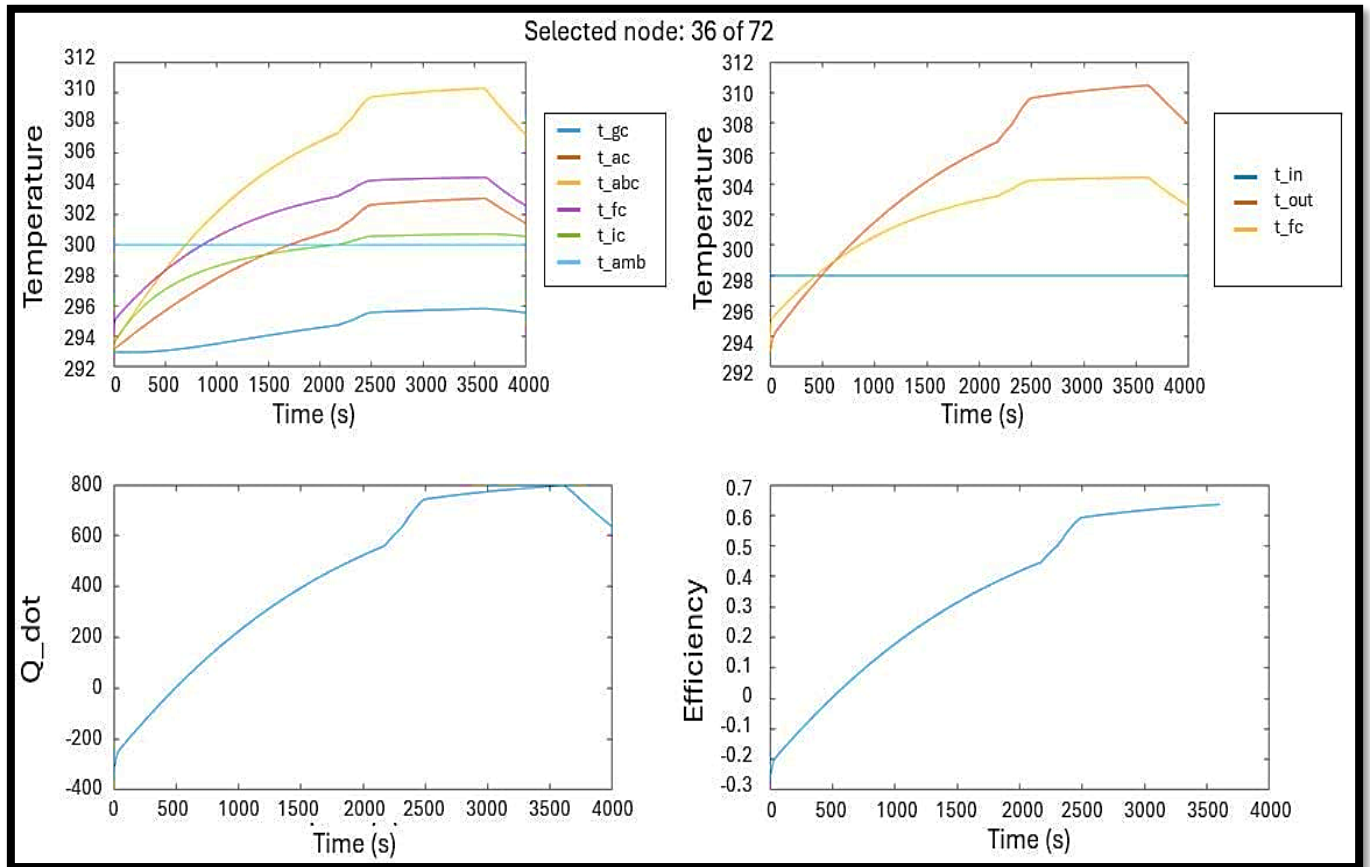


Figure 5 Type B: eff = 0.6357

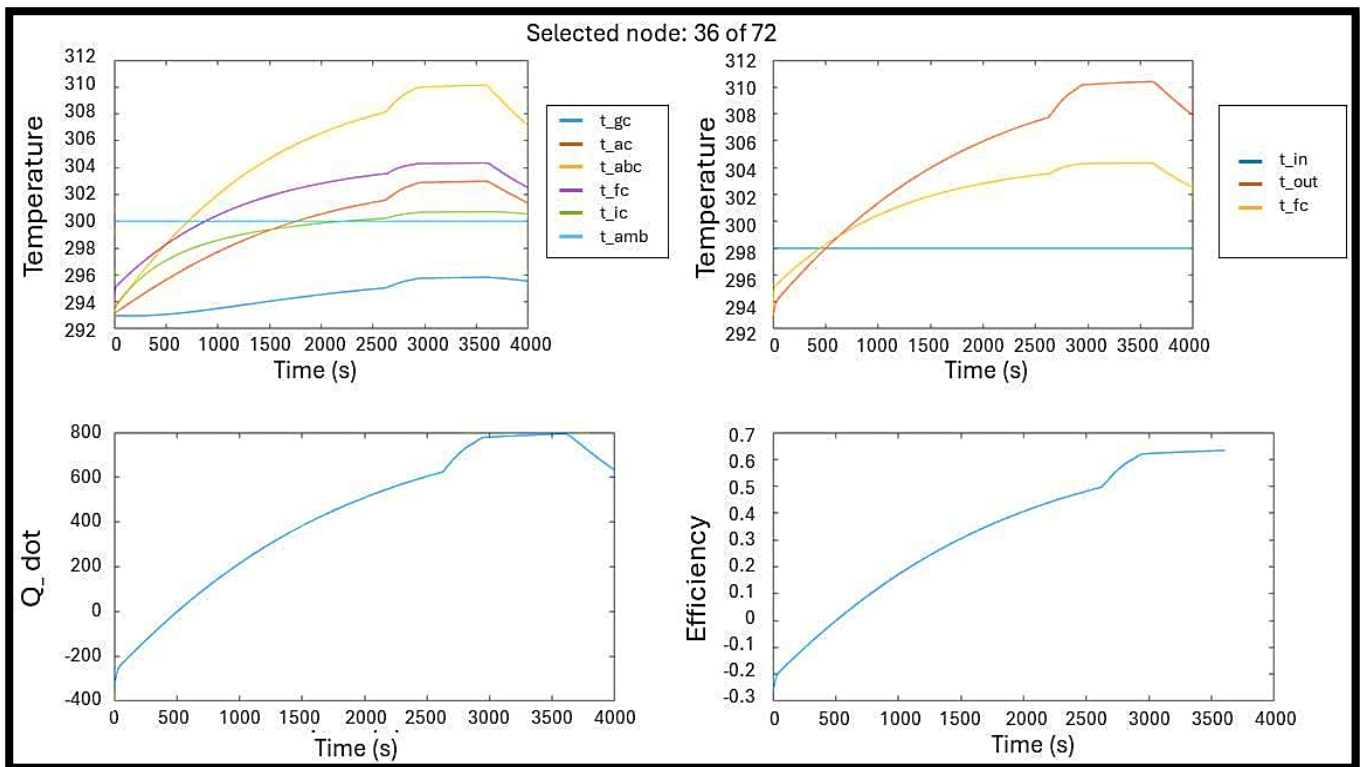


Figure 6 Type C: eff = 0.6333

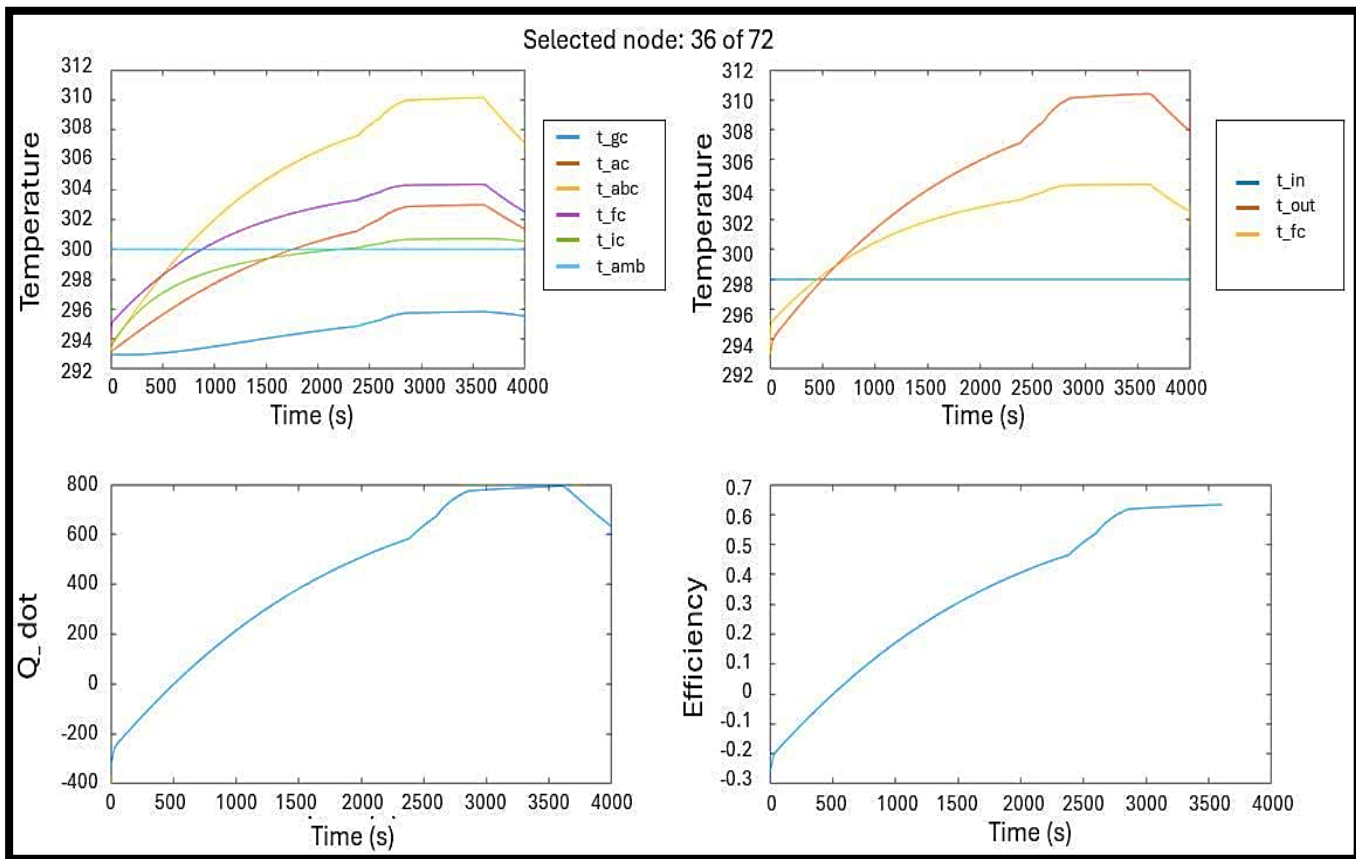


Figure 7 Type D: eff = 0.6332

Based on Figure 6, the Type C results are similar to the two previous types A and B. For the absorber temperatures on the upper left, the sequence of the temperatures from highest to lowest is: absorber (310.8 K), fluid, air gap, insulation, ambient, glass cover. Similarly, the temperatures of the fluid on the upper right side, the sequences of the temperatures from highest to lowest is: out (310.8 K), fluid, in. On the lower left, the highest heat obtained is almost 800 watts (W). Lastly, the efficiency on the lower right side reaches 63.33%.

From Figure 7, the results obtained in the Type D are similar to the three previous types A, B and C. In the upper left, which are the absorber temperatures, the temperatures are arranged in the following sequence (from highest to lowest): absorber (310.7 K), fluid, air gap, insulation, ambient, glass cover. In the upper right side, which are the temperatures of the fluid, the temperatures are arranged in the following sequence (from highest to lowest): out (310.7 K), fluid, in. In the lower left corner, the highest heat obtained is almost 800 watts (W). Lastly, on the lower right side, the efficiency reaches 63.32%.

From the four figures above (Figures 4 to 7), they show that the highest temperature in the SFPC occurs at the absorber, while in the fluid, it's found in the outlet. Table 4 shows the summary of the results of the Numerical Simulation.

As expected from four figures above (Figures 4 – 7) and Table 4, Type A has the highest absorber temperature obtained with 313.8 K, followed by Type B to D, which show that for the absorber temperature, there is only a difference of 2.9 K for the highest tri-colored (Type B) as compared with the black one. For the fluid temperature, the same thing happened, with Type A having the highest value with 313.8 K, followed by Type B to D. As observed,

the absorber temperature for all types (A to D), has the same temperature with the fluid outlet temperature. This means that the heat from the plate absorber is received all by the fluid coming out of the absorber. The difference in temperatures of the Types B to D is very small. Identical results happened also with the heat obtained (Q_{dot}), having the Type A with the highest with almost 1,000 watts (W), and with the three tri-colored types (B to D) almost has the same value of 800 W. And lastly, similar happened with the efficiency, with Type A having the highest efficiency with 80.32 %, while the tri-colored has 63.57%, 63.33 % and 63.32% efficiency, respectively. These show that the highest tri-colored absorber (Type B) lags behind with the black one with at least 16.75%.

Table 4 Summary of the results of the Numerical Simulation

| Parameters | Type A | Type B | Type C | Type D |
|------------------------------|--------|--------|--------|--------|
| Absorber Temperature (K) | 313.8 | 310.9 | 310.8 | 310.7 |
| Fluid outlet Temperature (K) | 313.8 | 310.9 | 310.8 | 310.7 |
| Heat Obtained, Q_{dot} (W) | 1,000 | 800 | 800 | 800 |
| Efficiency (%) | 80.32 | 63.57 | 63.33 | 63.32 |

The authors verify their obtained results through benchmarking against related literature (as from below), that is, the authors benchmark their results against those obtained by various authors of previously conducted studies. These comparisons help to verify that the new models produce consistent and reliable results.

In comparison to other studies, Nakoa et al. (2011) found that in March, the temperature of the water was 54 °C (327 K) for the black absorber, which is 13.2 K higher than our all black-Type A's 313.8 K. For the blue absorber, the temperature was 50 °C (323 K), which is 12.1 K higher than what we obtained for the highest tri-colored Type B's 310.9 K. The red-brown absorber yielded a temperature of 43 °C (316 K), and the colorless absorber produced a temperature of 41 °C (314 K) [19]. AlSaqoor (2014) reported that the black collector achieved the maximum temperature of water. The output temperature of water from the black absorber was 90 °C (363 K) which is 49.2 K higher than our Type A's 313.8 K, while it was 44 °C (317 K) for the light grey absorber, which is 6.1 K higher than our Type B's 310.9 K [13].

For the efficiency, Nakoa et al. determined the average monthly efficiency of the BSWH black absorber to be 57% in February and 56.5% in March. The 57% in February is 23.32% lower than what we achieved for our Type A's 80.32%. The blue absorber had an efficiency of 53% in February and 50% in March, in which the former is 10.57% lower than our Type B's 63.57%. The red brown absorber had an efficiency of 41% in February and 40% in March. Similarly, the colorless absorber had an efficiency of 35% in both February and March [19]. Anderson's theoretical and experimental studies indicated that the black absorber had the highest thermal efficiency of 64%, which is 16.32% lower than our Type A's 80.32%. The grey absorber had an efficiency of 59%, which is 4.57% lower than our Type B's 63.57%. Green and red absorbers had efficiencies of 53% and 44%, respectively, while the white absorber had an efficiency of 24% [7, 8].

The study conducted by Kalogirou et al. (2005) showed that colored solar collectors (with an absorptance of 0.85) performed only slightly worse (about 10% lower) than those with black absorbers (with an absorptance of 0.95), which is quite acceptable and comparable to our findings, with a difference of at least 16.75% (that is, our Type A with 80.32%, while Type B with 63.57%). However, collectors with black or color-selective coatings generated roughly 18% more thermal output than those that are simply painted. As evidenced by the results, colored collectors typically performed about 10% lesser than black collectors (whether painted normally or selectively), but the aesthetic improvement can outweigh this disadvantage [9].

In Salem's (2012) study, he evaluated the percentage of thermal energy produced by the colored absorbers compared to the black absorber. While the grey and green collectors generated nearly 40% of the total energy produced by black collectors, our tricolored absorbers Types B to D achieved 80% of the same value obtained by black one (that is, our Type A with 1,000 W, while Types B to D with 800 W) [5]. One noticeable is the data obtained by Tripanagnostopoulos et. al which showed that blue and red-brown absorbers resulted in about 15% lower efficiency compared to black absorbers, which is almost nearly identical to our 16.75% (that is, our Type A with 80.32%, while Type B with 63.57%) [4]. AlSaqoor's (2014) study revealed that the average efficiency of SFPC for black and light grey absorbers was found to be 55% and 12% respectively [13]. Our efficiency for Type A – black's 80.32% is 25.32% higher than his, while for light grey, our Type B's 63.57% is 51.57% higher than his. His black absorber had a capacity of an average value of 95 W, which is more than 900 W lesser than our Type A's 1,000 W, while the light grey absorber's capacity significantly decreased, reaching an average value of around 20 W, more than 700 W lower than our tri-colored's 800 W.

The verification can also be determined by the given and computed average solar absorptance of the four types of SFPC, based from solar absorptivity in Table 1. The average of the three colors' absorptivity is shown in Table 5 below. The table shows that the average absorptivity for each type coincides with the result of the simulation which is from Types A to D, arranged from highest to lowest.

Table 5 Average absorptivity.

| Type | Colors | Average Absorptivity |
|------|-------------------------------------|----------------------|
| A | All Black | 0.98 [58] |
| B | Dark Bronze, Award Blue, Teal Green | 75.5 |
| C | Burgundy, Award Blue, Teal Green | 74.88 |
| D | Burgundy, Award Blue, Dark Bronze | 74.85 |

3.2. Parametric Investigation Output

The following are the Output:

Output:

1. Irradiance – Transmitted $\{I_{transmitted}\}$ (W/m²)
2. Q useful $\{Q_{useful}\}$ (kW)
3. T hot $\{T_{hot}\}$ (°C)

Irradiance – Transmitted is the radiation that makes it into the collector. Q useful is the power delivered to the water tank, equal to the power received by the collector minus losses from the collector to the surroundings. T hot is the temperature of the hot portion of the solar storage tank volume. Figures 8 - 10 show the results of the Parametric Simulation. From the results of the Parametric investigation, the figures below show that the high heats (Q) and temperatures (T) obtained are usually happening during summer or dry season, with their peak values happening on the second week April, with the maximum Irradiance – transmitted at 930 W/m², with Q useful at 0.34 kW, and with highest T hot at 64 °C. On the other hand, cold or wet season gives low heats (Q) and temperatures (T), with their lowest values happening from mid-October to mid-November.

In March, the black absorber in the study of Nakoa et al., (2011) absorbed 542 W/m², which is 388 W/m² less than our 930 W/m². The blue absorber absorbed 448 W/m², the red brown absorbed 341 W/m², and the colorless absorbed 336 W/m² in the same study [19]. AlSaqoor's (2014) study found that black and light grey collectors absorbed 470 W/m², which is half (or 460 W/m²) of what we obtained 930 W/m² [13]. In the study of Sakhrieh and Al-Ghandoor's (2013), it indicates that the solar radiation intensity ranged from 154.0 to 1004.33 W/m², which is almost the same as our readings of 930 W/m² [14].

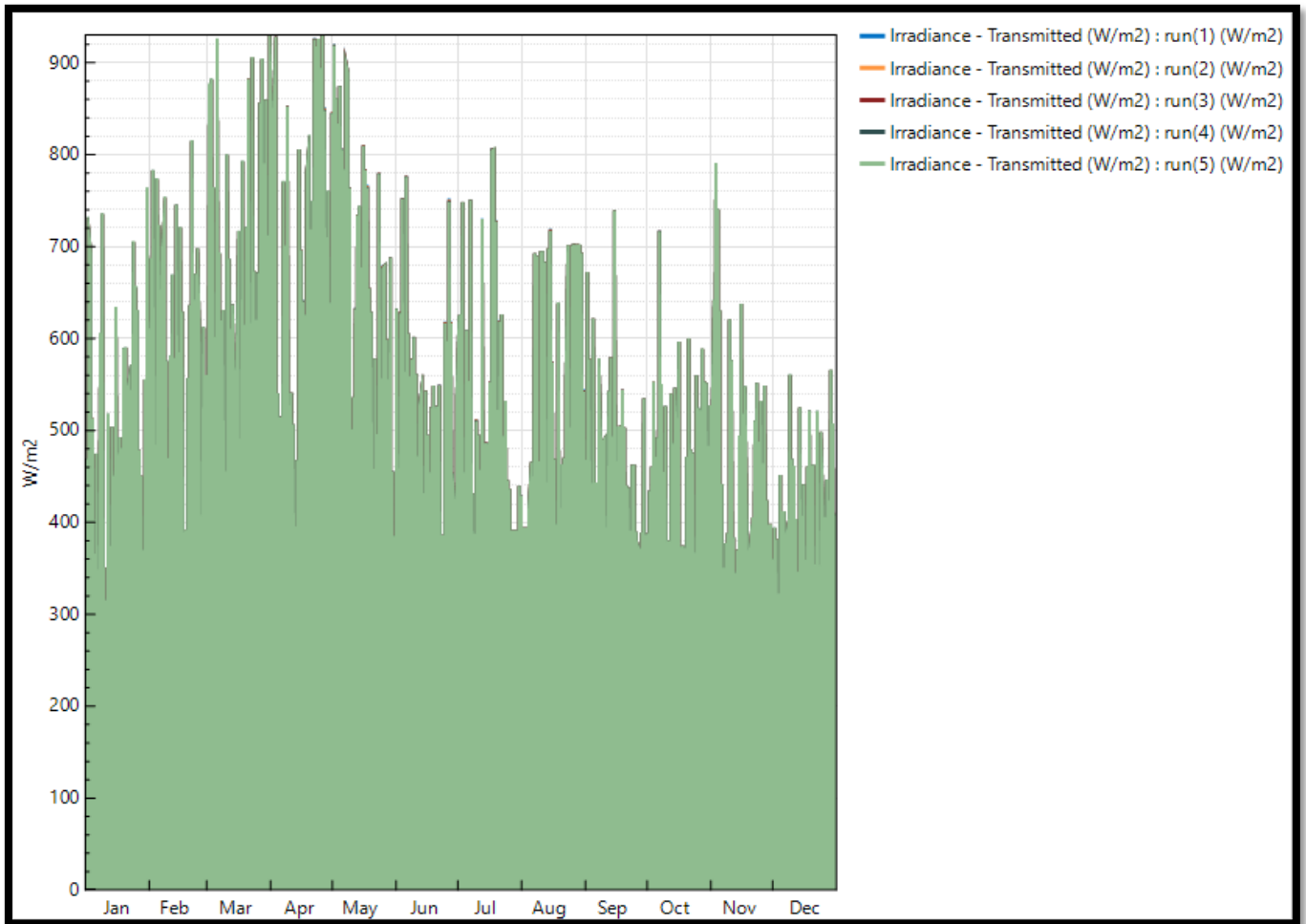


Figure 8 Irradiance – Transmitted

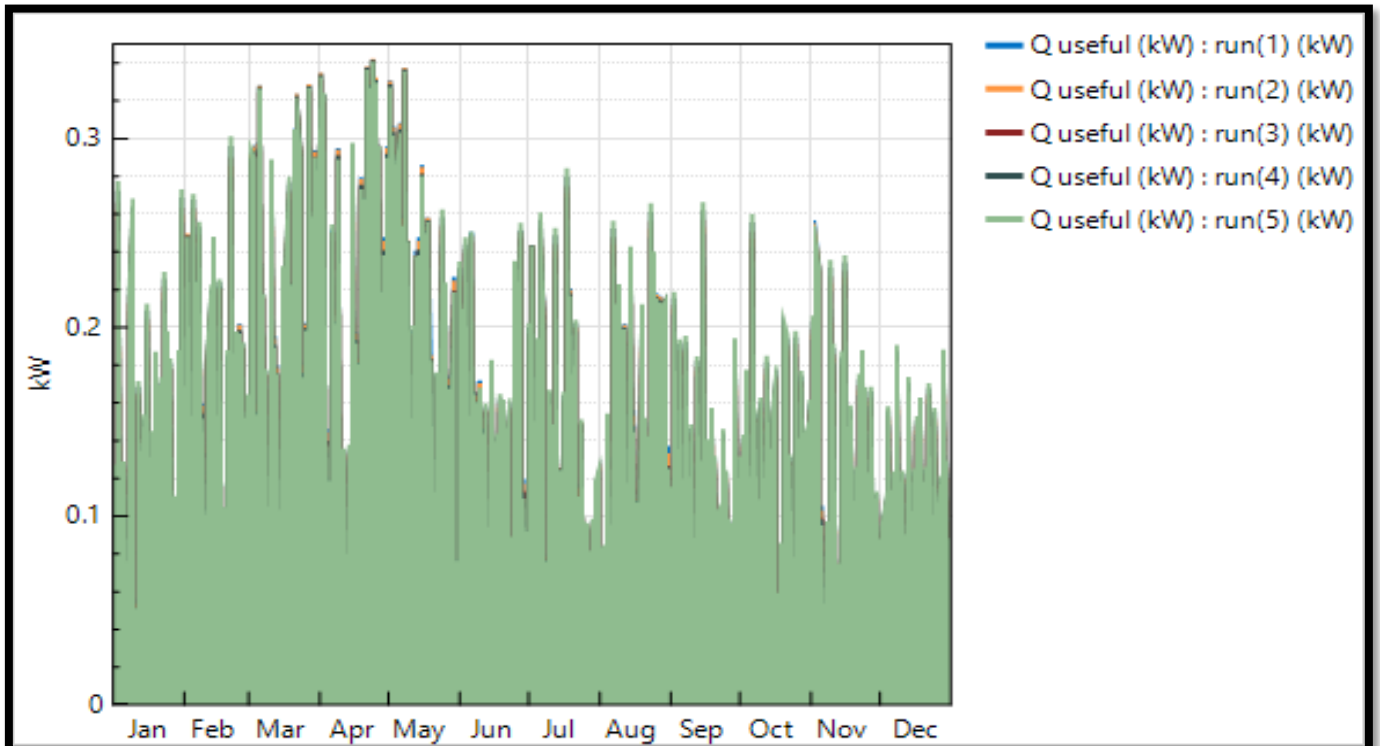


Figure 9 Q useful

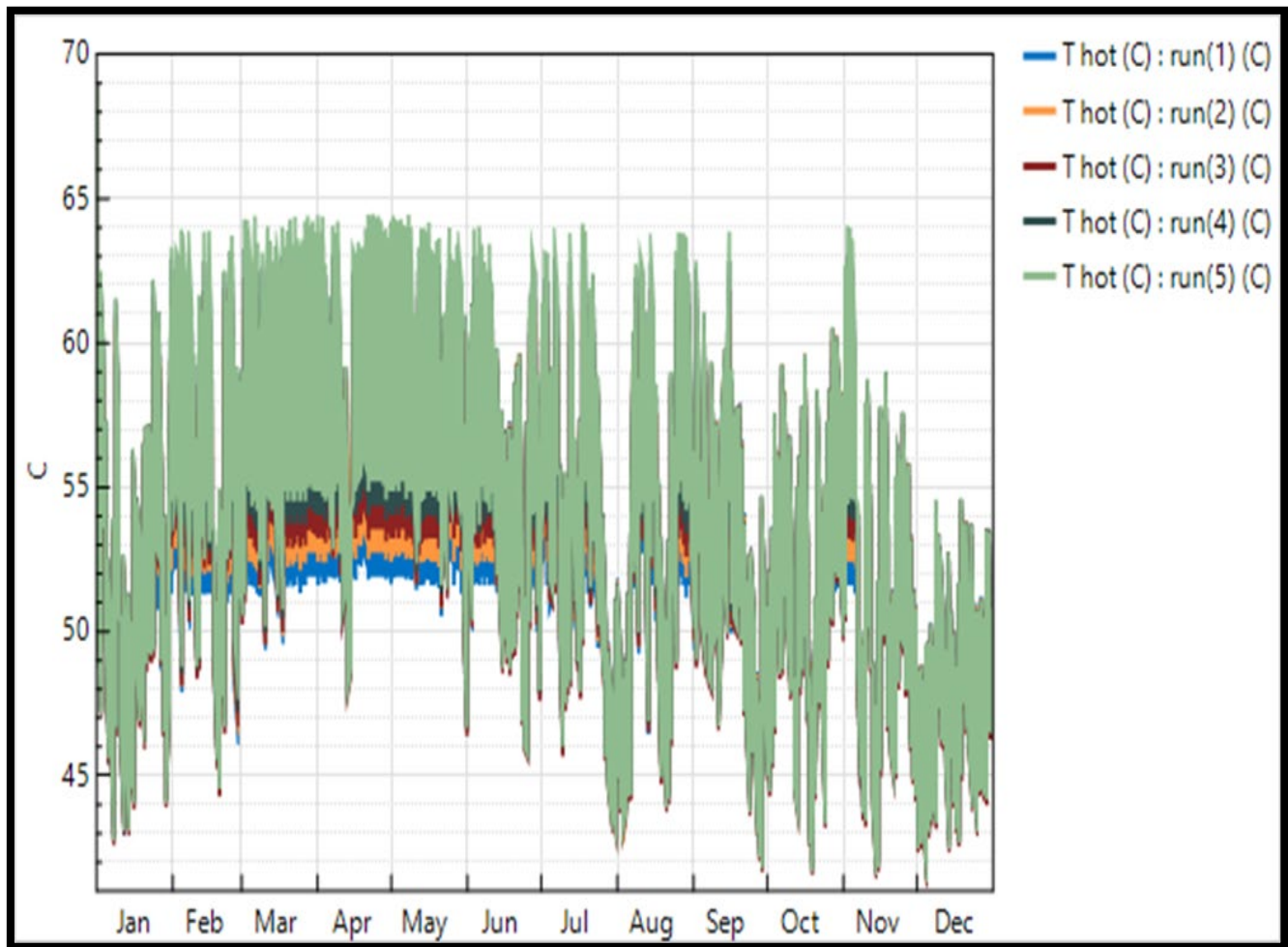


Figure 10 T hot

4.0 CONCLUSION

This study is conducted for a comparison between the use of black-colored collector or absorber and tri-colored ones. The researchers aim to determine the effects of the black color and to identify if the tri-colored collectors or absorbers could be an alternative to the black ones. It was found out that the temperatures of absorber and fluid out for the tri-colored differ with 2.9 K only as compared with the black absorber. Similarly, the heat obtained for tri-colored absorbers fell behind with the black one at least 200 W. Furthermore, the study also revealed that the black absorber has the highest efficiency of 80.32%, which was expected. Meanwhile, the tri-colored collectors lagged behind the black one with at least 16.75% efficiency, which could still be considered a good alternative to the black absorber.

Incorporating non-black absorbers into building architecture for functional and aesthetic reasons requires a number of future advancements to maximize efficiency while preserving aesthetic appeal. According to Duffy and Beckman (2013), scientists should concentrate on creating cutting-edge coatings and materials that have low thermal emittance and strong solar absorptance while coming in a range of hues [43]. Surface treatment innovations, including textured or nanostructured surfaces, can improve light-trapping properties and lower reflection losses, both of which are necessary to raise absorption rates [59]. Additional areas for improvement include: creating selectively reflective surfaces that

reflect unwanted wavelengths while absorbing desired ones [60]; enhancing insulation with cutting-edge materials and designs [61]; improving thermal management, which is another crucial area where advanced heat transfer materials and phase change materials (PCMs) are used [62]; using advanced computational modeling in conjunction with extensive experimental validation of different colors and coatings under various environmental conditions [45]; developing hybrid systems that combine non-black absorbers with other renewable technologies, like photovoltaic cells [63]; and optimizing system design, including the angle and orientation of collectors and integrating tracking systems [64].

By focusing on these strategies, future researches can develop non-black solar absorbers that are both efficient and aesthetically pleasing, facilitating their integration into building designs while maintaining high performance. Hence, despite having lower efficiency, the tri-colored absorbers can be taken into consideration for building integration. They can achieve an architecturally and visually pleasing result, avoiding the monotony of the black color and resulting in an aesthetically pleasing outcome. Additionally, they can also be integrated technically to meet the building's requirements.

Acknowledgement

This research is fully supported by Department of Science and Technology (DOST) – Engineering Research and Development for Technology (ERDT).

Conflicts of Interest

The author(s) declare(s) that there is no conflict of interest regarding the publication of this paper

References

- [1] Haque, Md & Bakshi, Arpita & Mobin, Fathum. 2021. Assessing The Factors Of Energy Consumption Behavior In Urban Area. *Journal of Civil Engineering, Science and Technology*. 12: 124-140. DOI: <https://doi.org/10.33736/jcest.3976.2021>
- [2] Amrutkar, S., Ghodke, S., and Patil, K. Solar flat plate collector analysis. *IOSR Journal of Engineering (IOSRJEN)*, 2(2): 207-213. DOI: <https://doi.org/10.9790/3021-0202207213>
- [3] Muhammad, M. J., Muhammad, I. A., Sidik, N. A. C., Yazid, M. N. A. W. M., Mamat, R. & Najafi, G. 2016."The use of nanofluids for enhancing the thermal performance of stationary solar collectors: A review. *Renewable and Sustainable Energy Reviews*, 63(C): 226-236. Elsevier DOI: 10.1016/j.rser.2016.05.063.
- [4] Tripanagnostopoulos, Y, Souliotis, M., and Nousia, T. 1999. Solar collectors with colored absorbers. *Solar Energy*, 68(4): 343-356. DOI: [https://doi.org/10.1016/S0038-092X\(00\)00031-1](https://doi.org/10.1016/S0038-092X(00)00031-1)
- [5] Salem, T. 2012. Colored absorbers for solar thermal collectors: A numerical study for Lebanese buildings. *2012 International Conference on Renewable Energies for Developing Countries (REDEC)*. DOI: <https://doi.org/10.1109/REDEC.2012.6416714>
- [6] Weiss, W., Stadler, I. 2001. Façade integration - a new and promising opportunity for thermal solar collectors. *Proceedings of the Industry Workshop of the IEA Solar Heating and Cooling Programme*, Task 26, 2001, Delft
- [7] Anderson, T., Duke, M., & Carson, J. 2010. The effect of colour on the thermal performance of building integrated solar collectors. *Solar Energy Materials and Solar Cells*, 94(2): 350-354. DOI: <https://doi.org/10.1016/j.solmat.2009.10.012>
- [8] Anderson, T., Duke, M., and Carson, J. 2009. Performance of coloured solar collectors. *The First International Conference on Applied Energy (ICAE09)*, (Hong Kong), January 2009.
- [9] Kalogirou, S., Tripanagnostopoulos, Y., & Souliotis, M. 2005. Performance of solar systems employing collectors with colored absorber. *Energy and Buildings*, 37(8), 824-835. DOI: <https://doi.org/10.1016/j.enbuild.2004.10.011>
- [10] Isac, L., Panait, R., Enesca, A., Bogatu, C., Perniu, D., & Duta, A. 2018, October. Development of black and red absorber coatings for solar thermal collectors. Nearly Zero Energy Communities, Springer *Proceedings in Energy*. DOI: https://doi.org/10.1007/978-3-319-63215-5_20
- [11] Perniu, D., Covei, M., Bogatu, C., Isac, L., Visa I., & Duta, A. 2020. Inorganic, coloured thin films for solar thermal energy convertors in sustainable buildings. *Energy Efficient Building Design*. 61-73, Springer, Cham. DOI: https://doi.org/10.1007/978-3-030-40671-4_4
- [12] Mueller, T., Wagner, W., Hausner, R., Koehl, M., Herkel, S., Orel, B., & Hoefler, K. 2004, July. Colourface - coloured facades for solar heating systems and building insulation. ISES Europe 2004 (EuroSun): *European Conference of the International Solar Energy Society (ISES)*, Freiburg im Breisgau, Germany.
- [13] ALSaqoor, S. 2014, April. The impact of aging and mechanical destruction on the performance of the flat plate solar collector in Tafila city climate in Jordan. *International Journal of Engineering Research and Application*. 4(4): 11-17.
- [14] Sakhrieh, A., & Al-Ghandoor, A. 2013. Experimental investigation of the performance of five types of solar collectors. *Energy Conversion and Management*, 65: 715-720. DOI: <https://doi.org/10.1016/j.enconman.2011.12.038>
- [15] Isac, L., Nicoara, L., Panait, R., Enesca, A., Perniu, D., & Duta, A. 2017, March. Alumina matrix with controlled morphology for colored spectrally selective coatings. *Environmental Engineering and Management Journal*, 16(3): 715-724. DOI: <https://doi.org/10.30638/eemj.2017.073>
- [16] Zheng, M., Wu, Y., Lin, L., Zheng, W., Qu, Y., & Lai, F. 2012. Design and analysis of colored solar selective absorbing films with three-layer structure. *Surface Review and Letters*, 19(5): 1250046 (7 pages). <https://doi.org/10.1142/S0218625X12500461>
- [17] Yang, R., Liu, J., Lin, L., Qu, Y., Zheng, W., & Lai, F. 2016. Optical properties and thermal stability of colored solar selective absorbing coatings with double-layer antireflection coatings. *Solar Energy*, 125: 453-459. DOI: <https://doi.org/10.1016/j.solener.2015.12.022>
- [18] Wu, Y., Zheng, W., Lin, L., Qu, Y., & Lai, F. 2013. Colored solar selective absorbing coatings with metal Ti and dielectric AlN multilayer structure. *Solar Energy Materials & Solar Cells*, 115: 145-150. DOI: <https://doi.org/10.1016/j.solmat.2013.03.041>
- [19] Nakoa, K. M. A., Karim, M. R., Mahmood, S. L., Akhanda, M. A. R. 2011. Effect of colored absorbers on the performance of a built-in-storage type solar water heater. *International Journal of Renewable Energy Research (IJRER)*, 232-239.
- [20] Orel, Z. C., Gunde, M. K., and Hutchins, M. G. 2005, January. Spectrally selective solar absorbers in different non-black colours. *Solar Energy Materials and Solar Cells*, 85(1): 41-50. DOI: <https://doi.org/10.1016/j.solmat.2004.04.010>
- [21] Orel, B., Spreizer, H., Vuk, A. S., Fir, M., Merlini, D., Vodlan, M., & Köhl, M. 2007. Selective paint coatings for coloured solar absorbers: Polyurethane thickness insensitive spectrally selective (TISS) paints (Part II). *Solar Energy Materials & Solar Cells*, 91: 108-119. DOI: <https://doi.org/10.1016/j.solmat.2006.07.012>
- [22] Orel, Z. C., & Gunde, M. K. 2000, April. Spectral selectivity of black and green painted surfaces. *Solar Energy Materials and Solar Cells*, 61 (4): 445 - 450. DOI: [https://doi.org/10.1016/S0927-0248\(99\)00155-5](https://doi.org/10.1016/S0927-0248(99)00155-5)
- [23] Zhu, D., Mao, F., & Zhao, S. 2012, March. The influence of oxygen in TiAlOxNy on the optical properties of colored solar-absorbing coatings. *Solar Energy Materials and Solar Cells*, 98: 179-184. DOI: <https://doi.org/10.1016/j.solmat.2011.11.001>
- [24] LinkedIn, 2024. *How many colors should you use in your design?* Accessed on March 26, 2024, from <https://www.linkedin.com/pulse/how-many-colors-should-you-use-your-design-laurie-bend/>
- [25] Tiger Color, 2021. "How many colors should you use in your designs?," 2021. Accessed on July 9, 2021, from <https://www.tigercolor.com/color-lab/tips/tip-01.html>.
- [26] Design Wizard, 2021. *80 Eye-Catching Color Combinations* For 2021. Accessed on March 26, 2024, from <https://designwizard.com/blog/colour-combination/>.
- [27] Duta, A., Isac, L., Milea, A., Ienei, E., & Perniu, D. 2014. Coloured solar-thermal absorbers - a comparative analysis of cermet structures. *Energy Procedia*, 48: 543 - 553.
- [28] Isac, L., Enesca, A., Mihoreanu, C., Perniu, D., & Duta, A. 2014. Spectrally solar selective coatings for colored flat plate solar thermal collectors. *Sustainable Energy in the Built Environment - Steps Towards nZEB, Springer Proceedings in Energy*. DOI: https://doi.org/10.1007/978-3-319-09707-7_21
- [29] Chen, F., Wang, S. W., Liu, X, Ji, R., Li, Z., Chen, X., Chen, Y., & Lu, W. 2016. Colorful solar selective absorber integrated with different colored units. *Optics Express*, 24(2): A92-103. doi: 10.1364/OE.24.000A92. PMID: 26832602. DOI: <https://doi.org/10.1364/OE.24.000A92>. PMID:26832602
- [30] Orel, B., Spreizer, H., Perše, L. S., Fir, M., Vuk, A. S., Merlini, D., Vodlan, M., & Köhl, M. 2007. Silicone-based thickness insensitive spectrally selective (TISS) paints as selective paint coatings for coloured solar absorbers (Part I). *Solar Energy Materials & Solar Cells*, 91: 93-107. DOI: <https://doi.org/10.1016/j.solmat.2006.07.013>
- [31] Wang, S.-W., Chen, F., Liu, X., Wang, X., Yu, L., & Lu, W. 2013. Colored solar-thermal absorbing coatings with high absorptance. *Optical Interference Coatings*. OSA Technical Digest (online) (Optical Society of America), paper MC.2. DOI: <https://doi.org/10.1364/OIC.2013.MC.2>
- [32] Zhao, S., Zhu, D., & Ribbing, C.-G. 2011, October. Colour control and selectivity in TiAlN solar-thermal absorbers. *Advances in Optical Thin Films IV. Proceedings of Society of Photo-Optical Instrumentation Engineers*. 8168, 81680G. DOI: <https://doi.org/10.1117/12.896591>

- [33] Zhu, D., & Zhao, S. 2010. Chromaticity and optical properties of colored and black solar-thermal absorbing coatings. *Solar Energy Materials & Solar Cells*, 94: 1630-163. DOI: <https://doi.org/10.1016/j.solmat.2010.05.019>
- [34] Dan, A., Chattopadhyay, K., Barshilia, H. C., & Basu, B. 2016. Colored selective absorber coating with excellent durability. *Thin Solid Films*. DOI: <https://doi.org/10.1016/j.tsf.2016.08.070>
- [35] Sarkar, A., Sinha, S., Palai, D., Dey, A., Mallick, A. B. 2018. Delineating the role of surface characteristics on the solar selectivity of colored chromium oxide coating on 304 stainless steel substrates. *Solar Energy Materials and Solar Cells*, 182: 354-361. <https://doi.org/10.1016/j.solmat.2018.03.043>
- [36] Mu, K., Kueh, A., Shek, P.N., Mohd Haniffah, M., & Tan, B. 2020. Flow responses alteration by geometrical effects of tubercles on plates under the maximal angle of attack. Proceedings of the Institution of Mechanical Engineers, Part C: *Journal of Mechanical Engineering Science*. 235: 3975 - 3987. DOI: <https://doi.org/10.1177/0954406220975434>
- [37] Mu, K., Kueh, A., & Shek, P. 2020. Hydroelastic responses of plates with sinusoidal tubercles under perpendicularly loaded flow. *Ocean Engineering*, 219: 108301. DOI: <https://doi.org/10.1016/j.oceaneng.2020.108301>
- [38] Kemarau, R. A., & Ebov, O. V. 2021. Study Influence Of Land Cover Change In Wetland And Vegetation On Land Surface Temperature. *Journal of Civil Engineering, Science and Technology*, 12(2): 66-74. DOI: <https://doi.org/10.33736/jcest.3970.2021>
- [39] [Houston Steel Buildings. 2020. *Metal Building Roof Colors and Solar Reflectance*. Retrieved on May 30, 2021, from <https://www.houstonsteelbuildings.net/single-post/2016/07/08/metal-building-roof-colors-and-solar-reflectance>
- [40] Saleh, A. May 2012. Modelling of flat-plate solar collector operation in transient states. (Doctoral dissertation), Purdue University, Fort Wayne, Indiana.
- [41] Saleh, Ahmad M., Mueller, Donald W., Abu-Mulaweh, Hosni I. 2013. [ASME 2013 International Mechanical Engineering Congress and Exposition - San Diego, California, USA (Friday 15 November 2013)] Volume 8B: Heat Transfer and Thermal Engineering - Flat-Plate Solar Collector in Transient Operation: Modeling and Measurements., V08BT09A036-. DOI: <https://doi.org/10.1115/IMECE2013-62377>
- [42] Zima, W., & Dziejawa, P. 2011. Modelling of liquid flat-plate solar collector operation in transient states. Proceedings of the Institution of Mechanical Engineers, Part A: *Journal of Power and Energy*, 225: 53-62. DOI: <https://doi.org/10.1177/09576509JPE1044>
- [43] Duffie, J. A., & Beckman, W. A. 2013. *Solar Engineering of Thermal Processes*. John Wiley & Sons. DOI: <https://doi.org/10.1002/9781118671603>
- [44] Kalogirou, S. A. 2004. Solar thermal collectors and applications. *Progress in Energy and Combustion Science*, 30(3): 231-295. DOI: <https://doi.org/10.1016/j.pecs.2004.02.001>
- [45] Prakash, J., & Garg, H. P. 2000. Performance evaluation of fixed and tracking solar energy concentrators. *Renewable Energy*, 19(1-2), 101-112.
- [46] System Advisor Model Version 2023.12.17 (SAM 2023.12.17 Revision 1, SSC 290). National Renewable Energy Laboratory. Golden, CO. Accessed May 10, 2024. <https://sam.nrel.gov/download>
- [47] System Advisor Model Version 2023.12.17 (SAM 2023.12.17 Revision 1, SSC 290) Website. 2024. Solar Water Heating. National Renewable Energy Laboratory. Golden, CO. Accessed May 29, 2024. <https://sam.nrel.gov/solar-water-heating.html>
- [48] Alternative Energy Tutorials. 2024. *Flat Plate Collector*. Retrieved on May 2, 2024, from <http://www.alternative-energy-tutorials.com/solar-hot-water/flat-plate-collector.html>
- [49] Rathi, Dushyant & Kumar, Arbind. 2016. Analytical study of the optimum mass flow rate of water in a natural circulation solar collector. *Carbon: Science and Technology*. 8: 103-111.
- [50] Solar365. 2024. *Pipe size and fluid volume in solar thermal systems*. Retrieved on May 30, 2024, from <http://www.solar365.com/solar/thermal/pipe-size-and-fluid-volume-solar-thermal-systems>
- [51] The Piping Engineering World. 2024. *Calculation of Insulation Thickness for Pipes*. Retrieved on June 2, 2024, from <https://www.pipingengineer.org/calculation-of-insulation-thickness-for-pipes/>
- [52] Buy Insulation Online. 2024. Nitrile Rubber Pipe Insulation. Retrieved on June 2, 2024, from <https://www.buyinsulationonline.co.uk/category/nitrile-rubber-section>
- [53] The Engineering ToolBox. 2024. *Insulated Copper Tubes - Heat Loss*. Retrieved on June 2, 2024, from https://www.engineeringtoolbox.com/copper-pipes-insulation-heat-loss-d_52.html
- [54] Comaklı, K., Cakır, U., Kaya, M., & Bakirci, K. 2012. The relation of collector and storage tank size in solar heating systems. *Energy Conversion and Management*, 63: 112-117. DOI: <https://doi.org/10.1016/j.enconman.2012.01.031>
- [55] Benhouia, A. T., Teggat, M., & Benchatti, A. 2018, March. Effect of sand as thermal damper integrated in flat plate water solar thermal collector. *International Journal of Heat and Technology*, 36(1): 21-25. <http://ijeta.org/Journals/IJHT>. DOI: <https://doi.org/10.18280/ijht.360103>
- [56] Meena, S., Meena, C. S. & Bajpai, V. K. 2014, March. Thermal performance of flat-plate collector: an experimental study. *International Journal of Engineering Research and Applications (IJERA)*. Special issue, 1-4 (A0104) National Conference on Advances in Engineering and Technology (AET). DOI: <https://doi.org/10.18485/aeletters.2018.3.4.3>
- [57] Skerlic, Jasmina & Nikolić, Danijela & Cvetković, Dragan & Mišković, Aleksandar. 2018. Optimal Position of Solar Collectors: A Review. *Applied Engineering Letters: Journal of Engineering and Applied Sciences*. 3: 129-134. DOI: <https://doi.org/10.18485/aeletters.2018.3.4.3>
- [58] Solar Mirror. 2024. Table of absorptivity and emissivity of common materials and coatings. Retrieved on June 2, 2024, from <http://www.solarmirror.com/fom/fom-serve/cache/43.html>
- [59] Chopra, K. L., Paulson, P. D., & Dutta, V. 2004. Thin-film solar cells: an overview. *Progress in Photovoltaics: Research and Applications*, 12(2-3): 69-92. DOI: <https://doi.org/10.1002/pip.541>
- [60] Granqvist, C. G. 2007. Transparent conductors as solar energy materials: A panoramic review. *Solar Energy Materials and Solar Cells*, 91(17): 1529-1598. DOI: <https://doi.org/10.1016/j.solmat.2007.04.031>
- [61] Kalogirou, S. A. 2004. Solar thermal collectors and applications. *Progress in Energy and Combustion Science*, 30(3): 231-295. DOI: <https://doi.org/10.1016/j.pecs.2004.02.001>
- [62] Sharma, A., Tyagi, V. V., Chen, C. R., & Buddhi, D. 2009. Review on thermal energy storage with phase change materials and applications. *Renewable and Sustainable Energy Reviews*, 13(2): 318-345. DOI: <https://doi.org/10.1016/j.rser.2007.10.005>
- [63] Kumar, R., & Rosen, M. A. 2011. Integrated collector-storage solar water heater with extended storage unit. *Energy Conversion and Management*, 52(3): 1767-1773. DOI: <https://doi.org/10.1016/j.applthermaleng.2010.09.021>
- [64] Hestnes, A. G. 1999. Building integration of solar energy systems. *Solar Energy*, 67(4-6): 181-187. DOI: [https://doi.org/10.1016/S0038-092X\(00\)00065-7](https://doi.org/10.1016/S0038-092X(00)00065-7)